Volume 40
Number 17
August 13, 2001

Inorganic Chemistry
including bioinorganic chemistry

Articles

Ligand Dependence of Metal−Metal Bonding in the d^3d^3 Dimers $M_2X_9^{n-}$ (M^{III} = Cr, Mo, W; M^{IV} = Mn, Tc, Re; X = F, Cl, Br, I)

Robert Stranger,* Alison Turner, and Christopher D. Delfs

Department of Chemistry, The Faculties, The Australian National University, Canberra, ACT 0200 Australia

Received December 29, 2000

The ligand dependence of metal−metal bonding in the d^3d^3 face-shared $M_2X_9^{n-}$ (M^{III} = Cr, Mo, W; M^{IV} = Mn, Tc, Re; X = F, Cl, Br, I) dimers has been investigated using density functional theory. In general, significant differences in metal−metal bonding are observed between the fluoride and chloride complexes involving the same metal ion, whereas less dramatic changes occur between the bromide and iodide complexes and minimal differences between the chloride and bromide complexes. For M = Mo, Tc, and Re, change in the halide from F to I results in weaker metal−metal bonding corresponding to a shift from either the triple metal−metal bonded to single bonded case or from the latter to a nonbonded structure. A fragment analysis performed on $M_2X_9^{3-}$ (M = Mo, W) allowed determination of the metal−metal and metal-bridge contributions to the total bonding energy in the dimer. As the halide changes from F to I, there is a systematic reduction in the total interaction energy of the fragments which can be traced to a progressive destabilization of the metal-bridge interaction because of weaker $M-X_{bridge}$ bonding as fluoride is replaced by its heavier congeners. In contrast, the metal−metal interaction remains essentially constant with change in the halide.

Introduction

Metal−metal interactions ranging from weak magnetic coupling through to multiple metal−metal bonding are often important in understanding the novel magnetic and catalytic properties exhibited in dimeric and polynuclear metal complexes.[1] The calculation of the electronic structure of these systems, however, still remains a challenge to theoretical chemists. Despite enormous developments in computational chemistry, quantum chemical calculations on open-shell bimetallic systems using state-of-the-art ab initio molecular-orbital methods are formidable because of the high level of electron correlation often necessary to describe the ground-state wave function.[2] This in particular applies to the optimization of the geometries of such systems. In a series of recent papers,[3] however, we have shown that the combination of density functional theory with the broken-symmetry (BS) approach of Noodleman et al.[4] to modeling magnetically coupled metal clusters is a reliable method for calculating structures of open-shell bimetallic complexes over a large range of metal−metal interactions. Unlike other methods that employ the full symmetry of the dimer, thereby forcing the magnetic electrons to be delocalized over both metal centers, the BS approach makes no assumption regarding the extent of delocalization. Thus, the BS approach is able to encompass both the weakly coupled (localized) and strong metal−metal bonded (delocalized) limits as well as all intermediate situations, making it an ideal tool to study periodic trends in metal−metal bonding.

* To whom correspondence should be addressed.

(1) Cotton, F. A.; Walton, R. A. *Multiple Bonds Between Metal Atoms*, 2nd ed.; Oxford University Press: New York, 1993; and references therein.

(2) (a) Hall, M. B. *Polyhedron* **1987**, *6*, 679. (b) Bénard, M. In *Quantum Chemistry−Basic Aspects, Actual Trends*; Carbo, R., Ed.; Elsevier: Amsterdam, 1989. (c) Siegbahn, P. E. M. *Adv. Chem. Phys.* **1996**, *93*, 333.

(3) (a) Lovell, T.; McGrady, J. E.; Stranger, R.; Macgregor, S. A. *Inorg. Chem.* **1996**, *35*, 3079. (b) McGrady, J. E.; Stranger, R.; Lovell, T. *Inorg. Chem.* **1997**, *36*, 3242. (c) McGrady, J. E.; Stranger, R.; Lovell, T. *J. Phys. Chem. A* **1997**, *101*, 6265. (d) McGrady, J. E.; Stranger, R.; Lovell, T. *Inorg. Chem.* **1998**, *37*, 3802. (e) Stranger, R.; McGrady, J. E.; Lovell, T. *Inorg. Chem.* **1998**, *37*, 6795. (f) Stranger, R.; Lovell, T.; McGrady, J. E. *Inorg. Chem.* **1999**, *38*, 5510. (g) Stranger, R.; Lovell, T.; McGrady, J. E. *Inorg. Chem.* **2001**, *40*, 39.

(4) (a) Noodleman, L.; Norman, J. G., Jr. *J. Chem. Phys.* **1979**, *70*, 4903. (b) Noodleman, L. *J. Chem. Phys.* **1981**, *74*, 5737. (c) Noodleman, L.; Case, D. A. *Adv. Inorg. Chem.* **1992**, *38*, 423.

10.1021/ic001476m CCC: $20.00
Published on Web 07/19/2001

Our initial work focusing on the d^3d^3 face-shared dimers $M_2Cl_9^{n-}$ (M^{III} = Cr, Mo, W; M^{IV} = Re) revealed that the BS approach was capable of reproducing the known metal−metal separations to within 0.1 Å.[3a−c] On the other hand, if full-symmetry methods were used, metal−metal separations were underestimated by as much as 1 Å in the case of the weakly coupled chromium system. Since then, we have successfully used this approach to optimize the geometries of a number of structurally characterized d^1d^1, d^2d^2, and d^3d^3 face-shared and edge-shared dimer systems, and in all cases, the calculated structures are in good agreement with the experimental data.[3e−g] Recently, the same approach has also been shown to be applicable in accommodating the effects of internal rotation in quadruply metal−metal bonded dimers.[5] It should be noted that although the BS state does not correspond to the true singlet ground state, the latter can be obtained using spin-projection techniques. However, we have previously shown that the potential-energy curve projected for the singlet state closely follows the BS curve, and therefore, the geometries optimized for the BS state are expected to correspond closely to those of the ground-state singlet.[3c]

On the basis of the diverse range of metal−metal separations found in face-shared $M_2X_9^{n-}$ complexes,[6] it would be reasonable to assume that the μ-X_3 entity is a very flexible bridging unit allowing the structure of the dimer to be determined largely by the electronic properties of the component metal ions. However, this assumption is not supported by our earlier calculations on $Mo_2Cl_9^{3-}$ and $W_2Cl_9^{3-}$ which showed that the metal−bridge interaction is not only in opposition to the metal−metal interaction but in fact is the major contribution to the total interaction energy.[7] As the size of the bridge atoms increase, it is anticipated that direct metal−metal interactions will be further constrained, and this is borne out by the structural data available for the series $Cs_3Mo_2X_9$ (X = Cl, Br, I), where change in the halide from chlorine to bromine to iodine is associated with 0.16 and 0.25 Å increases in the metal−metal separation, respectively.[6b]

The experimental data for the $Mo_2X_9^{3-}$ (X = Cl, Br, I) series clearly indicate that altering the bridging unit can bring about significant structural changes with consequent effects on metal−metal bonding.[6c] Accordingly, we intend to investigate these ligand effects more closely by undertaking a detailed study of the ligand dependence of metal−metal bonding in the series of d^3d^3 complexes $M_2X_9^{n-}$ with M^{III} = Cr, Mo, W; M^{IV} = Mn, Tc, Re; and X = F, Cl, Br, I.

Computational Details

All approximate density functional calculations reported in this work were performed on Linux-Pentium III (600 MHz) computers using the 1999 version of the Amsterdam Density Functional (ADF) program developed by Baerends et al.[8] A triple-ζ Slater type orbital basis set extended with a single d-polarization function was used to describe the halide atoms, whereas all metals atoms were modeled with a triple-ζ basis set. Electrons in orbitals up to and including 1s {F}, 2p {Cl}, 3p {Br, Cr, Mn}, 3d {Mo, Tc}, 4p {I}, and 4d {W, Re} were treated in accordance with the frozen-core approximation. Geometry optimizations were performed using the gradient algorithm of Versluis and Ziegler.[9]

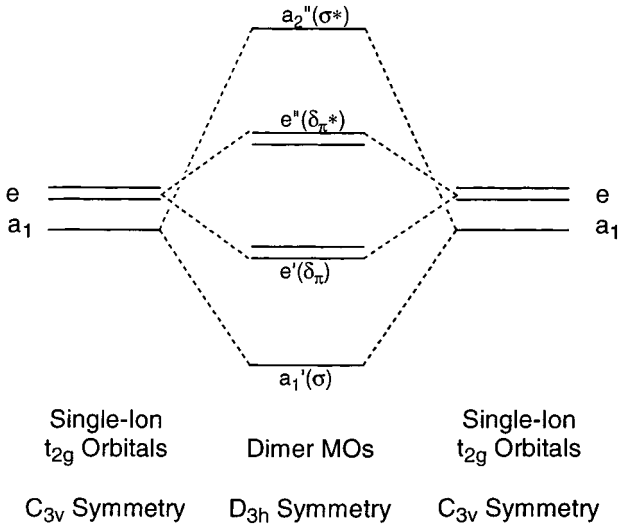

Figure 1. Contribution of the single-ion trigonal (C_{3v} symmetry) d orbitals to the molecular orbitals (D_{3h} symmetry) involved in metal−metal bonding in face-shared $M_2X_9^{n-}$ dimers.

Calculations on the $M_2X_9^{n-}$ dimers were performed in an unrestricted manner using D_{3h} and C_{3v} symmetry for the full- and broken-symmetry (BS) calculations, respectively. For the BS calculations, all symmetry elements connecting the two metal centers were removed and an initial asymmetry in spin density was introduced using the modifystartpotential key. The LDA approximation was used employing the local exchange-correlation potential of Vosko et al.[10] Neither gradient or relativistic corrections were applied in the geometry optimizations as they have been shown to result in generally poorer agreement with the crystallographically determined structures than those of the LDA in isolation, particularly in relation to the metal−metal separation.[3c] The potential-energy curves for the BS and S = 0, 2 and 3 associated states were generated by freezing the metal−metal separation, rM−M, at 0.1 Å intervals and optimizing all other independent structural parameters. For the fragment interaction analysis, energies were calculated incorporating the gradient corrections of Becke and Perdew[11] but using the above LDA optimized geometries obtained for the BS state.

Results and Discussion

As in previous work, our discussion of the metal−metal bonding in the above face-shared $M_2X_9^{n-}$ systems will be undertaken through a detailed analysis of the BS potential-energy curves in terms of the corresponding curves for the S = 0, 2, and 3 associated states. The associated states correspond to different occupations of the metal−metal bonding and antibonding orbitals depicted in Figure 1 which are based on the full (D_{3h}) symmetry of the dimer. These molecular orbitals are derived from symmetric and antisymmetric combinations of the trigonal (C_{3v}) t_{2g}-based single-ion orbitals of a_1 and e

(5) Lledos, A.; Jean, Y. *Inorg. Chem.* **1998**, *37*, 3321.
(6) (a) Cotton, F. A.; Ucko, D. A. *Inorg. Chim. Acta* **1972**, *6*, 161. (b) Stranger, R.; Grey, I. E.; Madsen, I. C.; Smith, P. W. *J. Solid State Chem.* **1987**, *69*, 162. (c) Stranger, R.; Smith, P. W.; Grey, I. E. *Inorg. Chem.* **1989**, *28*, 1271.
(7) Stranger, R.; Macgregor, S. A.; Lovell, T.; McGrady, J. E.; Heath, G. A. *J. Chem. Soc., Dalton Trans.* **1996**, 4485.
(8) (a) Baerends, E. J.; Bérces, A.; Bo, C.; Boerrigter, P. M.; Cavallo, L.; Deng, L.; Dickson, R. M.; Ellis, D. E.; Fan, L.; Fischer, T. H.; Fonseca Guerra, C.; van Gisbergen, S. J. A.; Groeneveld, J. A.; Gritsenko, O. V.; Harris, F. E.; van den Hoek, P.; Jacobsen, H.; van Kessel, G.; Kootstra, F.; van Lenthe, E.; Osinga, V. P.; Philipsen, P. H. T.; Post, D.; Pye, C.; Ravenek, W.; Ros, P.; Schipper, P. R. T.; Schreckenbach, G.; Snijders, J. G.; Sola, M.; Swerhone, D.; te Velde, G.; Vernooijs, P.; Versluis, L.; Visser, O.; van Wezenbeek, E.; Wiesenekker, G.; Wolff, S. K.; Woo, T. K.; Ziegler, T. *Amsterdam Density Functional*, 1999 ed.; 1999. (b) Fonseca Guerra, C.; Snijders, J. G.; te Velde, G.; Baerends, E. J. *Theor. Chem. Acc.* **1998**, *99*, 391.
(9) Versluis, L.; Ziegler, T. J. *Chem. Phys.* **1988**, *88*, 322.
(10) Vosko, S. H.; Wilk, L.; Nusair, M. *Can. J. Phys.* **1980**, *58*, 1200.
(11) (a) Becke, A. D. *Phys. Rev. A* **1988**, *38*, 3098. (b) Perdew, J. P. *Phys. Rev. B* **1986**, *33*, 8822. (c) Perdew, J. P. *Phys. Rev. B* **1986**, *34*, 7406. (d) Perdew, J. P.; Chekavry, J. A.; Vosko, S. H.; Jackson, K. A.; Pederson, M. R.; Singh, D. J.; Fioihais, C. *Phys. Rev. B* **1992**, *46*, 6671.

Scheme 1

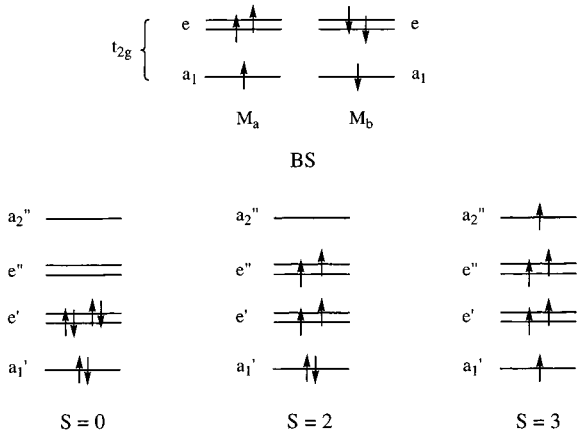

symmetry which have σ and δ_π ($^2/_3\delta + {}^1/_3\pi$) character, respectively, relative to the trigonal axis of the dimer. The associated states arise from successive decoupling (unpairing) of the σ and δ_π subsets of magnetic electrons and in each case can be represented by a single-determinant wave function, corresponding to the electron configurations shown in Scheme 1, where the weakly coupled electrons are ferromagnetically aligned.

Irrespective of the extent of delocalization of the σ and δ_π electrons, the BS state can always be specified in C_{3v} symmetry by the antiferromagnetic configuration $(a_1\uparrow)^1(a_1\downarrow)^1(e\uparrow)^2(e\downarrow)^2(a_1\uparrow)^0(a_1\downarrow)^0(e\uparrow)^0(e\downarrow)^0$ shown in Scheme 1. However, depending on which subsets of electrons are involved in weak magnetic coupling (localized) or strong metal−metal bonding (delocalized), three distinct coupling regimes can be recognized for the BS potential-energy curve as the metal−metal separation is reduced. To ascertain which description is applicable at each point along the BS curve, use is made of the associated states because, when antiferromagnetic coupling of a particular subset of electrons is weak, the associated state in which the weakly coupled electrons are ferromagnetically aligned must also lie close in energy. Accordingly, when all electrons are weakly coupled, the $S = 3$ state will lie close to the BS curve, whereas when only the δ_π electrons are weakly coupled, the $S = 2$ state will lie closest. Finally, when all electrons are strongly coupled, the BS state will converge with the $S = 0$ state where complete delocalization of the electrons is enforced. Each of the coupling schemes described above will only be valid over a limited range of metal−metal distances corresponding to where the potential-energy curve for the relevant associated state lies parallel and close in energy to the BS curve. Thus, the nature of the metal−metal bonding in each complex can be ascertained simply by inspection of the potential-energy curves and will reflect the coupling scheme occurring in the associated state which lies closest to the global minimum in the BS curve.

Potential-energy curves showing the dependence of the total energy on the metal−metal separation are plotted for the BS and $S = 0$, 2, and 3 associated states in Figures 2−6, for selected complexes. The optimized metal−metal separations and total energies for the BS and $S = 0$, 2, and 3 associated states for all complexes examined in this study are given in Table 1. Total energies for the associated states are given relative to the BS state. The charges on the metal and the terminal and bridging halides for each complex are given in Table 2, based on a Hirshfeld charge analysis of the BS state. Irrespective of the halide involved, the charge on the metal always remains low, below +0.5 units. A progressive reduction in the metal charge

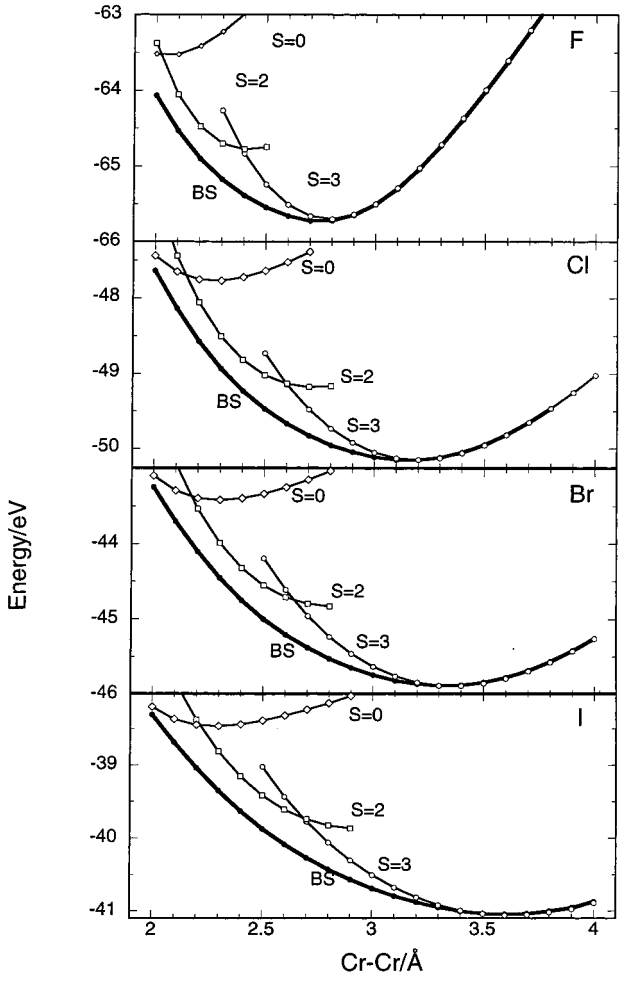

Figure 2. Potential-energy curves as a function of the metal−metal separation, rM−M, for the broken-symmetry (BS) and $S = 0$, 2, and 3 associated states of $Cr_2X_9^{3-}$ (X = F, Cl, Br, I).

is observed as F is replaced by the heavier halides Cl, Br, and I, with most $M_2I_9^{n-}$ dimers, except for $Cr_2I_9^{3-}$ and $Mo_2I_9^{3-}$, having small negative charges on the metals. The variation in charge on the metal is largely compensated for by the change in charge on the bridging halides, with the most dramatic differences occurring between the fluoride and chloride complexes of each metal system. In contrast, the charge on the terminal halides remains relatively constant with change in the halide, particularly for the Cr triad. For the nonaiodide complexes of the Mn triad, the bridging halides actually have positive charges, albeit very small, no greater than +0.05.

The uncorrected and covalency-corrected spin-densities on the metal, based on a Mulliken population analysis, are also tabulated in order to provide an indication of the degree of metal−metal bonding in each complex. The covalency-corrected spin-density corresponds to the unpaired spin-density on the metal in the absence of metal−ligand covalency effects and is obtained by scaling the uncorrected value by the factor $3.0/\rho^*$ where ρ^* is the calculated spin density on each metal for the $S = 3$ state where all electrons are unpaired and therefore weakly coupled. The deviation of ρ^* from 3.0 can be attributed entirely to covalency effects as the metal-based electrons in the $S = 3$ state do not participate in any metal−metal bonding. The covalency-corrected spin density gives a more realistic picture of the number of electrons on the metal participating in weak antiferromagnetic coupling. This is best illustrated for $Tc_2I_9^{1-}$, where the uncorrected value of 2.06 and covalency-corrected

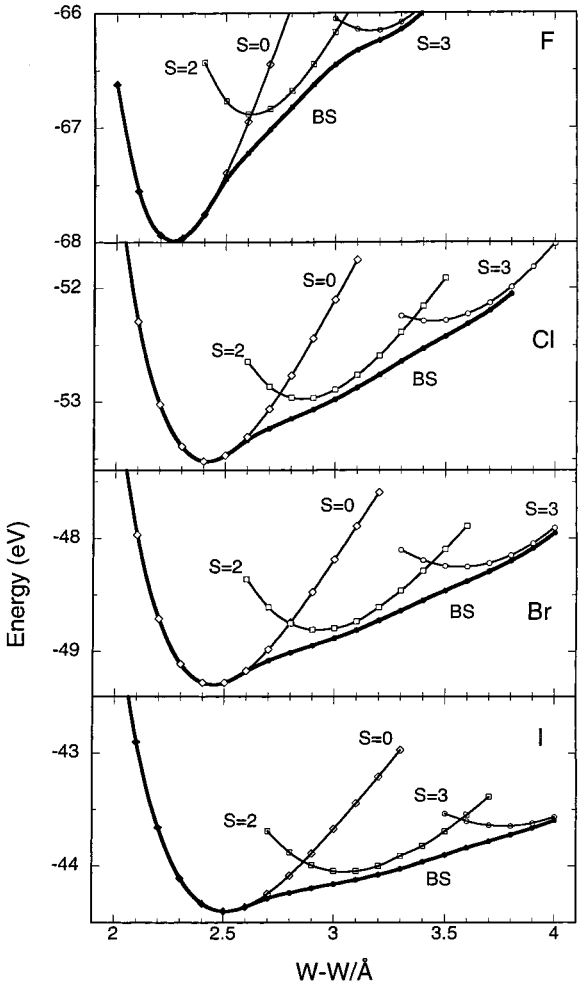

Figure 3. Potential-energy curves as a function of the metal−metal separation, rM−M, for the broken-symmetry (BS) and $S = 0$, 2, and 3 associated states of $W_2X_9^{3-}$ (X = F, Cl, Br, I).

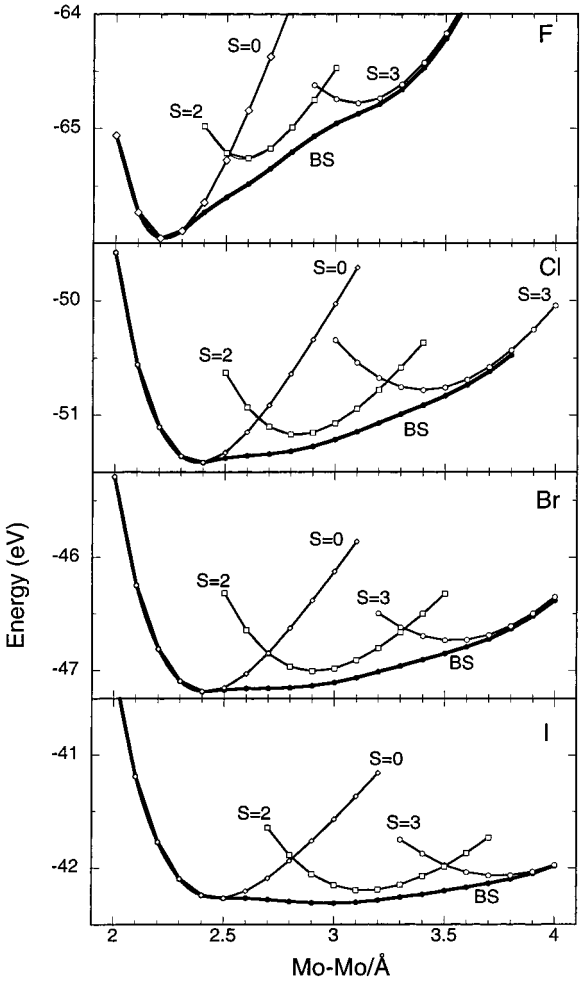

Figure 4. Potential-energy curves as a function of the metal−metal separation, rM−M, for the broken-symmetry (BS) and $S = 0$, 2, and 3 associated states of $Mo_2X_9^{3-}$ (X = F, Cl, Br, I).

value of 2.95 differ by nearly one whole electron. Thus, on the basis of the uncorrected value, it would be reasonable to assume that the complex possesses a metal−metal bond as there appears to be only two unpaired electrons on each Tc ion. The covalency-corrected value on the other hand indicates that no metal−metal bond exists as all three electrons on each Tc center remain unpaired. The latter description is certainly more consistent with the very large metal−metal separation of approximately 3.7 Å calculated for the BS state.

Potential-Energy Curves. A cursory glance at the potential-energy curves in Figures 2−6 reveals that the most significant differences involving the same metal ion are observed between the fluoride and chloride complexes with less dramatic changes occurring between bromide and iodide and minimal differences between chloride and bromide. For the chromium, manganese, and tungsten complexes, change in the halide from F to I produces no overall change in the nature of the metal−metal bonding in the BS state. In contrast, for the molybdenum, technetium, and rhenium complexes, change in the halide from F to I results in the description of the metal−metal bonding in the BS state corresponding to a weaker coupling arrangement, namely, a shift from the triple ($\sigma + 2 \times \delta_\pi$) metal−metal bonded to single (σ) bonded case for both the molybdenum and rhenium systems and from the latter to a nonbonded structure for the technetium system. It is also noted that the minima for the associated states occur at progressively larger metal−metal separations, rM−M, as the halide is changed from F through to I. This trend reflects the smaller size of the fluoride ion and hence its ability to allow more compressed bioctahedral structures.

$Cr_2X_9^{3-}$ and $Mn_2X_9^{1-}$. The potential-energy curves for the $Cr_2X_9^{3-}$ system are shown in Figure 2. From Table 1, the calculated metal−metal distances of 2.76, 3.12, and 3.29 Å in the BS state for $Cr_2X_9^{3-}$ (X = F, Cl, Br) are in excellent agreement with the crystallographically determined values of 2.77, 3.12, and 3.32 Å, respectively.[12a,e,i] To date, there are no crystallographic or magnetic data reported for any $Mn_2X_9^{1-}$ complex. However, we note that the calculated metal−metal separations for the $Mn_2X_9^{1-}$ dimers are consistently shorter than their $Cr_2X_9^{3-}$ analogues by as much as 0.1 Å. Optimized metal−metal distances for the BS state are calculated between 2.65 and 3.65 Å with the largest differences occurring between the chloride and fluoride complexes. For both $Cr_2X_9^{3-}$ and $Mn_2X_9^{1-}$ systems, the energetic ordering of the minima for the associated states is $S = 3 < S = 2 < S = 0$. The minimum for the $S = 3$

(12) (a) Wessel, G. J.; Ijdo, D. J. W. *Acta Crystallogr.* **1957**, *10*, 466. (b) Watson, W. H., Jr.; Waser, J. *Acta Crystallogr.* **1958**, *11*, 689. (c) Saillant, R.; Wentworth, R. A. D. *Inorg. Chem.* **1968**, *7*, 1606. (d) Grey, I. E.; Smith, P. W. *Aust. J. Chem.* **1971**, *24*, 73. (e) Saillant, R.; Jackson, R. B.; Streib, W. E.; Folting, K.; Wentworth, R. A. D. *Inorg. Chem.* **1971**, *10*, 1453. (f) Dunbar, K. R.; Pence, L. E. *Acta Crystallogr. C* **1991**, *47*, 23. (g) Heath, G. A.; McGrady, J. E.; Raptis, R. G.; Willis, A. C. *Inorg. Chem.* **1996**, *35*, 6838. (h) Nissen, S. C. Ph.D. Thesis, Australian National University, 1997. (i) Schenker, R.; Heer, S.; Güdel, H. V.; Weihe, H. *Inorg. Chem.* **2001**, *40*, 1482.

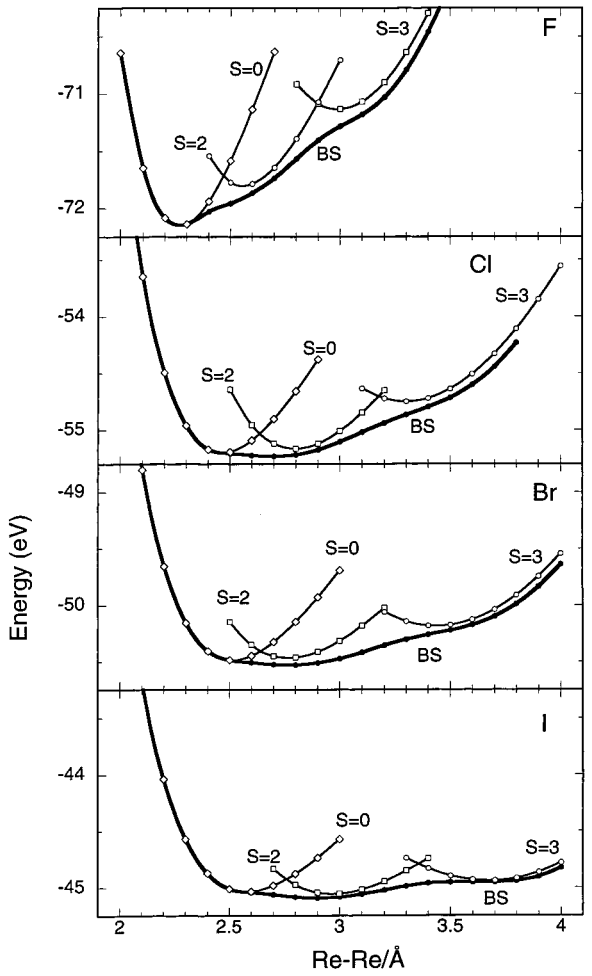

Figure 5. Potential-energy curves as a function of the metal−metal separation, rM−M, for the broken-symmetry (BS) and $S = 0$, 2, and 3 associated states of $Re_2X_9^{1-}$ (X = F, Cl, Br, I).

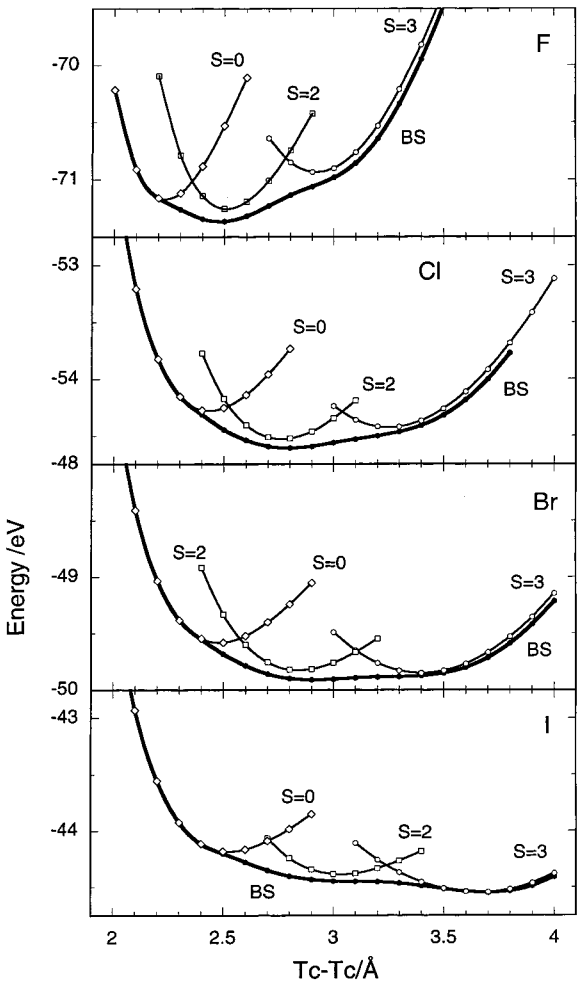

Figure 6. Potential-energy curves as a function of the metal−metal separation, rM−M, for the broken-symmetry (BS) and $S = 0$, 2, and 3 associated states of $Tc_2X_9^{1-}$ (X = F, Cl, Br, I).

state lies well below those for $S = 0$ and 2 and is observed to converge with the minimum in the BS curve indicating that both σ and δ_π subsets of electrons are weakly coupled in the BS state. This description of the coupling is consistent with the covalency-corrected spin densities which are all very close to 3.0, and also with the weak antiferromagnetic exchange reported for $Cr_2X_9^{3-}$ (X = F, Cl, Br) complexes.[12c,d,i]

$W_2X_9^{3-}$. In stark contrast with the Cr and Mn systems discussed above, the potential-energy curves for the $W_2X_9^{3-}$ system shown in Figure 3 are indicative of very strong metal−metal bonding with the minimum in each of the BS curves located between 2.25 and 2.55 Å. The calculated W−W separation for $W_2Cl_9^{3-}$ is in excellent agreement with the published crystallographic value of 2.41 Å for $K_3W_2Cl_9$.[12b] For each complex, the energetic ordering of the associated states, namely, $S = 0 < S = 2 < S = 3$, is the reverse of that found for the Cr and Mn analogues. The global minimum in the BS curve for each complex is observed to converge with the curve for the $S = 0$ state below 2.5 Å where strong metal−metal triple bonding prevails, accounting for the temperature-independent magnetic behavior reported for $W_2Cl_9^{3-}$.[12b,f] Although the ordering of the associated states remains constant for all $W_2X_9^{3-}$ complexes, a progressive stabilization of the $S = 2$ and 3 spin states relative to $S = 0$ occurs as the halide changes from F through to I. Consequently, for the iodide complex the BS curve is observed to take on a more flattened appearance. Once again, the most dramatic change in the relative energies of the associated states and thus the BS curve is observed on passing from the fluoride to chloride complex. In particular, the significant stabilization of the $S = 0$ state relative to $S = 2$ and 3 by over 1 eV in the fluoride complex undergoes an abrupt change to around 0.5 eV in the chloride. In contrast, the energetic separation of the $S = 2$ and 3 states remains relatively unchanged (ca. 0.7 eV).

$Mo_2X_9^{3-}$ and $Re_2X_9^{1-}$. The similarity of the potential-energy curves for the $Mo_2X_9^{3-}$ and $Re_2X_9^{1-}$ systems shown in Figures 4 and 5, respectively, highlight the diagonal relationship between these two metals in the periodic table. For both systems, change in the halide from F to I sees the metal−metal bonding progress from a strong triple bond at short metal−metal separations between 2.2 and 2.3 Å in the fluoride complexes to a single bond at intermediate metal−metal distances around 3.0 Å in the iodide complexes. Again, the calculated metal−metal distances for the BS state in $Mo_2X_9^{3-}$ (X = Cl, Br, I) and $Re_2X_9^{1-}$ (X = Cl, Br) are in very good agreement with the reported crystallographic values.[7a,12e,g] In the fluoride complexes, the potential-energy curves for the associated states are well separated energetically in the order $S = 0 < S = 2 < S = 3$. Thus, the minimum in the BS curve corresponds to complete delocalization of the metal-based electrons in a metal−metal triple bond. In the iodide complexes, however, the potential-energy curves for all three associated states are similar in energy leading to relatively flat potential-energy curves for the BS state over a wide range of metal−metal distances between 2.5 and

Table 1. Relevant Structural Data and Energies of Minima for Broken-Symmetry (BS) and Associated States in $M_2X_9^{n-}$ (M^{III} = Cr, Mo, W; M^{IV} = Mn, Tc, Re; X = F, Cl, Br, I) Complexes

		energy (eV) and rM−M (Å) at minima[a]							
		BS		$S = 0$		$S = 2$		$S = 3$	
M	X	E_{tot}	rM−M	E_{rel}	rM−M	E_{rel}	rM−M	E_{rel}	rM−M
Cr	F	−65.73	2.755	2.19	2.049	0.95	2.416	0.03	2.789
	Cl	−50.15	3.119	2.38	2.270	0.97	2.714	0.00	3.187
	Br	−45.88	3.285	2.46	2.299	1.05	2.843	−0.01	3.338
	I	−41.04	3.650	2.58	2.279	1.17	2.952	−0.02	3.607
Mo	F	−65.96	2.213	0.00	2.215	0.70	2.578	1.18	3.086
	Cl	−51.41	2.380	0.00	2.378	0.24	2.828	0.63	3.399
	Br	−47.19	2.610	0.00	2.410	0.18	2.899	0.45	3.537
	I	−42.31	3.000	0.04	2.471	0.12	3.053	0.24	3.726
W	F	−67.99	2.252	0.00	2.250	1.11	2.611	1.84	3.163
	Cl	−53.52	2.400	0.00	2.398	0.55	2.849	1.24	3.429
	Br	−49.29	2.440	0.00	2.444	0.48	2.926	1.04	3.563
	I	−44.40	2.531	0.00	2.509	0.35	3.020	0.75	3.761
Mn	F	−70.00	2.647	2.98	2.146	1.20	2.360	0.02	2.649
	Cl	−51.86	3.093	2.75	2.406	1.23	2.790	0.00	3.087
	Br	−47.04	3.278	2.71	2.412	1.17	2.868	0.00	3.299
	I	−41.48	3.559	b	b	b	b	0.01	3.535
Tc	F	−71.36	2.478	0.19	2.220	0.10	2.504	0.43	2.928
	Cl	−54.61	2.800	0.33	2.443	0.08	2.757	0.19	3.248
	Br	−49.91	2.901	0.33	2.484	0.08	2.840	0.06	3.390
	I	−44.55	3.697	0.37	2.507	0.17	2.895	0.01	3.653
Re	F	−72.15	2.263	0.00	2.258	0.35	2.553	1.02	3.000
	Cl	−55.23	2.665	0.03	2.460	0.07	2.791	0.48	3.287
	Br	−50.53	2.785	0.04	2.513	0.06	2.867	0.35	3.412
	I	−45.08	2.933	0.04	2.574	0.03	2.998	0.15	3.610

[a] Energies for $S = 0$, 2, and 3 associated states are given relative to BS state. [b] Unable to be calculated.

Table 2. Results of a Population and Charge Analysis for the BS State in $M_2X_9^{n-}$ (M^{III} = Cr, Mo, W; M^{IV} = Mn, Tc, Re; X = F, Cl, Br, I) Complexes[a]

M	X	ρ	ρ_{corr}	Q_M	Q_{Xb}	Q_{Xt}
Cr	F	2.90	2.98	0.36	−0.33	−0.46
	Cl	3.01	2.97	0.27	−0.24	−0.47
	Br	3.11	2.98	0.24	−0.22	−0.47
	I	3.29	2.98	0.17	−0.20	−0.46
Mo	F	0.00	0.00	0.30	−0.35	−0.43
	Cl	0.00	0.00	0.21	−0.26	−0.44
	Br	0.00	0.00	0.17	−0.23	−0.45
	I	2.09	2.31	0.09	−0.16	−0.45
W	F	0.00	0.00	0.13	−0.30	−0.39
	Cl	0.00	0.00	0.00	−0.21	−0.40
	Br	0.00	0.00	−0.03	−0.17	−0.40
	I	0.00	0.00	−0.11	−0.12	−0.40
Mn	F	2.62	2.99	0.34	−0.15	−0.20
	Cl	2.68	2.99	0.06	−0.05	−0.16
	Br	2.82	2.99	0.01	−0.02	−0.16
	I	2.99	2.99	−0.08	0.02	−0.15
Tc	F	1.82	2.21	0.39	−0.17	−0.21
	Cl	1.75	2.38	0.08	−0.04	−0.17
	Br	1.81	2.44	0.01	0.00	−0.17
	I	2.06	2.95	−0.13	0.02	−0.13
Re	F	0.00	0.00	0.41	−0.20	−0.20
	Cl	1.40	1.96	0.09	−0.06	−0.17
	Br	1.51	2.11	0.02	−0.01	−0.17
	I	1.45	2.13	−0.12	0.05	−0.16

[a] ρ and ρ_{corr} correspond to the uncorrected and covalency-corrected spin densities on the metal determined from a Mulliken population analysis. Q_M, Q_{Xb}, and Q_{Xt} are the calculated charges on the metal, bridging, and terminal halides, respectively, based on a Hirshfeld charge analysis.

4.0 Å. The global minimum in the BS curve for $Re_2I_9^{1-}$ is almost coincident with the minimum for the $S = 2$ state, and therefore, the description of the coupling in this complex corresponds most closely to that of a metal−metal σ bond but weakly coupled δ_π electrons, in agreement with the corrected spin density of approximately 2.1 on each of the metals. A similar description of the metal−metal bonding applies to $Re_2Cl_9^{1-}$ and $Re_2Br_9^{1-}$ as corrected spin densities of approximately 2 are found for both complexes. This description of the magnetic coupling is in accord with magnetic measurements[12h] on the tetrabutylammonium salt of $Re_2Br_9^{1-}$ where moderately strong antiferomagnetic coupling was observed based on the reported value of the exchange coupling constant, $-J_{ab}$, of approximately 200 cm^{-1}. In the case of $Mo_2I_9^{3-}$, however, the global minimum in the BS curve is not coincident with the $S = 2$ curve. The corrected spin density on each molybdenum ion is approximately 2.3, and therefore, the description of the coupling is intermediate between that of a metal−metal single (σ) bonded and a nonbonded structure but clearly much closer to the former. For $Mo_2Cl_9^{3-}$ and $Mo_2Br_9^{3-}$, the BS minimum converges with the $S = 0$ curve, and therefore, both complexes are best described as possessing a metal−metal triple bond. However, the minima for the $S = 2$ curve is energetically very close (approximately 0.2 eV), and this has a significant impact on the magnetic and structural properties exhibited by these complexes as discussed below.

For the $Mo_2X_9^{3-}$ system, the energetic separation of the associated states is progressively reduced as X changes from Cl to Br to I, but at all times, the ordering remains as $S = 0 < S = 2 < S = 3$. In the case of the Re system, however, the $S = 0$ and 2 states are approximately equienergetic for the same three halide complexes, indicating that the metal−metal bonding is weaker, and this is supported by the smaller exchange coupling constant of $-J_{ab} = 200$ cm^{-1} reported for $Re_2Br_9^{1-}$ compared to approximately 380 cm^{-1} for $Mo_2Br_9^{3-}$.[6c,12h] Thus, whereas the global minimum in the BS curve corresponds to a metal−metal triple bonded structure for the F, Cl, and Br complexes of $Mo_2X_9^{3-}$, in the case of $Re_2X_9^{1-}$, only the fluoride complex possesses a metal−metal triple bond. Overall, the contracted nature of the 5d orbitals in Re^{4+} leads to much weaker metal−metal bonding in $Re_2X_9^{1-}$ compared to the other third row transition-metal system $W_2X_9^{3-}$ which exhibits metal−metal triple bonded structures for all four halide complexes.

We have discussed the potential-energy curves for $Mo_2Cl_9^{3-}$ in a previous communication.[3c] In the present work, however, the improved basis sets on both the metal and halide atoms have resulted in a much flatter BS curve over metal−metal separations between 2.4 and 2.9 Å. Consequently, although the minimum in the BS curve is found at approximately 2.4 Å, it is very shallow, and a distinctive plateau region is observed between 2.5 and 2.9 Å. A similar plateau region is also observed in the BS curve for the bromide complex. The fact that this plateau region in both $Mo_2Cl_9^{3-}$ and $Mo_2Br_9^{3-}$ lies less than 500 cm^{-1} above the BS minimum and within easy reach once consideration is made for solid-state packing and thermal effects has direct relevance in understanding the unusual magnetic and structural changes that occur in the $A_3Mo_2X_9$ (X = Cl, Br) system with change in the counterion, A.[6b,c] As the size of the counterion is varied, the $Mo_2Cl_9^{3-}$ anion is observed to undergo a systematic elongation corresponding to an increase in the metal−metal separation of approximately 0.3 Å from the K^+ through to the Me_4N^+ salt with a concomitant decrease in the exchange coupling constant, $-J_{ab}$, from 560 to 275 cm^{-1}. For the analogous bromide complexes, the difference in metal−metal distance spans over 0.5 Å for the same series of cations. The range of metal−metal separations over which this elonga-

tion occurs experimentally corresponds closely to the plateau regions observed in the calculated BS potential-energy curves in Figure 4. Over this range of metal−metal distances, the ground-state coupling in both complexes varies between that of a metal−metal triple-bonded structure toward 2.5 Å and a metal−metal single bond closer to 2.9 Å. Thus, the systematic reduction in $-J_{ab}$ for these complexes with increasing size of the cation can be attributed to a progressive decoupling of the δ_π subset of electrons because of the increasing metal−metal separation.

$Tc_2X_9^{1-}$. For the $Tc_2X_9^{1-}$ system, change in the halide results in the metal−metal bonding varying from a single bond in the case of $Tc_2F_9^{1-}$ to no metal−metal bonding for $Tc_2I_9^{1-}$. The energetic ordering of the associated states for $Tc_2F_9^{1-}$ is $S = 0 \sim S = 2 < S = 3$, and the global minimum in the BS curve at 2.5 Å lies closest to the $S = 2$ state corresponding to a metal−metal σ bonded structure. This description of the coupling is essentially in agreement with the corrected spin density of approximately two unpaired electrons on each Tc center. For $Tc_2Cl_9^{1-}$, the $S = 2$ curve still lies closest to the BS minima, but the corrected spin density of approximately 2.4 indicates that the complex is intermediate between a metal−metal single bonded and a nonbonded structure but closer to the former. For $Tc_2I_9^{1-}$, the ordering changes to $S = 0 > S = 2 > S = 3$, and consequently, the global minimum in the BS curve now occurs at a large metal−metal separation of 3.7 Å, indicative of weak coupling of both σ and δ_π subsets of electrons. For the Br complex, the BS curve exhibits a shallow double minimum structure, with the minima positioned at approximately 2.9 and 3.4 Å almost equienergetic. At the metal−metal separation of 2.9 Å, the corrected spin density on the metal is very similar to that found for the Cl complex, and therefore, the BS state is best described as intermediate between a metal−metal σ bonded and a nonbonded structure. For the other minimum at around 3.4 Å, the $S = 3$ curve lies closest to the BS curve, and accordingly, the BS state at this metal−metal separation corresponds to a weakly coupled d^3d^3 system. Given that the two minima are separated by less than 0.05 eV, the metal−metal bonding in the Br complex is predicted to be very sensitive to environmental effects such as solid-state packing. Preliminary magnetic studies[12h] on $(Bu_4N)Tc_2Br_9$ reveal that the $Tc_2Br_9^{1-}$ complex exhibits weak antiferromagnetism with a room-temperature magnetic moment of 3.78 μ_B, indicative of approximately three unpaired electrons on each metal center. The observed magnetic behavior is consistent with the structure adopting an equilibrium metal−metal separation in the vicinity of the second calculated minimum at 3.4 Å. For the Cl, Br, and I complexes, it is noted that the separation of the $S = 2$ and 3 associated states is less than 0.15 eV, and consequently, the BS curves for all three complexes appear relatively broad and flat over a large range of metal−metal distances, particularly for the Br and I complexes. As found for Re^{4+}, the contracted nature of the 4d orbitals in Tc^{4+} results in weaker metal−metal bonding in the $Tc_2X_9^{1-}$ system relative to the analogous second row transition-metal system involving Mo^{3+}. Thus, unlike $Mo_2X_9^{3-}$, which possesses metal−metal triple bonds for both the F and Cl complexes, the strongest metal−metal bonding which occurs in the $Tc_2X_9^{1-}$ system is at most only a metal−metal σ bond.

Fragment Analysis. We have previously undertaken a density functional study[7] of the metal−metal and metal−bridge interactions and ligand steric repulsion effects in $M_2Cl_9^{3-}$ (M = Mo, W) using a fragment approach.[13] These calculations, which were performed for $S = 0-3$ dimer spin states, revealed that the metal−bridge interaction is not only in opposition to the direct metal−metal interaction but, in fact, is the largest contribution to the total interaction energy. In the present study, we intend to compliment the previous work by investigating the effect of changing the bridging halide on the total bonding energy of the dimer. In an analogous fashion, we will make use of the fragment approach employed previously where the metal−metal interaction energy can be ascertained from constructing the $\{M_2X_6\}$ fragment from two $\{MX_3\}$ units. Subsequent formation of the complete $[M_2X_9]^{3-}$ dimer by combining the $\{M_2X_6\}$ and $\{X_3\}^{3-}$ fragments then allows the determination of the metal−bridge interaction in isolation. The total interaction energy of the fragments is obtained by combining two terminal $\{MX_3\}$ fragments with the bridging $\{X_3\}^{3-}$ unit and in principle should equate to the sum of the metal−metal and metal-bridge interaction energies. In the calculations, the geometries of the $\{MX_3\}$ and $\{X_3\}^{3-}$ fragments corresponded to those obtained from the BS calculations on the $M_2X_9^{3-}$ dimers. Calculations on the $\{MX_3\}$ fragments and $M_2X_9^{3-}$ dimers were performed in a spin-unrestricted manner, whereas those on the $\{X_3\}^{3-}$ fragments were spin-restricted.[14] In all cases, the gradient corrections of Becke and Perdew[11] were incorporated in calculating the total energy. In constructing the $\{M_2X_6\}$ fragments, the two $\{MX_3\}$ units were positioned such that the metal−metal distance was maintained at the value found in the BS state of the $M_2X_9^{3-}$ dimer.

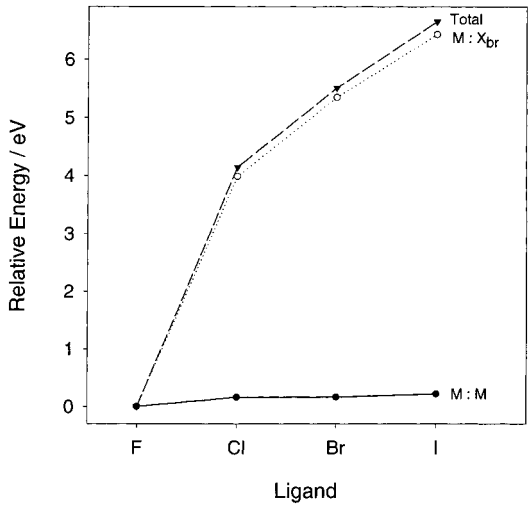

Figure 7. Metal−metal (M:M), metal−bridge ($M:X_{br}$), and total interaction energies for $Mo_2X_9^{3-}$ (X = F, Cl, Br, I) relative to the fluoride complex.

The metal−metal, metal−bridge, and total interaction energies, along with the energy associated with the formation of the terminal MX_3 fragments, are given in Table 3 as a function of both the halide and metal (Mo, W). The dependence of the metal−metal, metal−bridge, and total interaction energies on the halide in the $Mo_2X_9^{3-}$ system is shown in Figure 7 relative to the fluoride complex. Clearly, as the halide changes from fluoride through to iodide, there is a systematic reduction in the total interaction energy and a concomitant increase in the metal−metal separation. The largest variation in the total interaction energy occurs when fluorine is substituted with

(13) Ziegler, T. *NATO ASI., Ser. C* **1992**, *378*, 367.

(14) Spin restricted calculations were used to generate the MX_3 fragments, and a correction was applied to the total bonding energy which corresponded to the difference between the bond energy of spin restricted MX_3 and spin unrestricted MX_3 fragments as described in ADF1999 userguide.

Table 3. Fragment Interaction Energies for $M_2X_9^{3-}$ (M = Mo, W; X = F, Cl, Br, I) complexes

		interaction energy/kJ mol^{-1}			
	M−M/Å	MX_3	$\{X_3M\}-\{MX_3\}$	$\{M_2X_6\}-\{X_3\}^{3-}$	$\{X_3M\}-\{X_3\}^{3-}-\{MX_3\}$
			$Mo_2X_9^{3-}$		
X = F	2.015	−1843	−232	−1495	−1727
X = Cl	2.297	−1322	−224	−1051	−1275
X = Br	2.333	−1174	−240	−889	−1129
X = I	2.389	−984	−246	−777	−1023
			$W_2X_9^{3-}$		
X = F	2.251	−1964	−291	−1496	−1787
X = Cl	2.415	−1442	−292	−1088	−1380
X = Br	2.445	−1288	−294	−941	−1235
X = I	2.506	−1099	−294	−821	−1115

chlorine and this concurs with the earlier description of the BS potential-energy curves where the greatest difference was observed between the fluoride and chloride dimers. In contrast, the metal−metal interaction energy remains essentially constant with change in the halide even though the metal−metal separation increases by 0.26 and 0.37 Å for the $W_2X_9^{3-}$ and $Mo_2X_9^{3-}$ systems, respectively, as fluorine is replaced with iodine. This implies that any decrease in metal−metal interaction resulting from the larger halides forcing the dimer to become more elongated is compensated for by the increasing dilation of the metal d orbitals because of metal−ligand covalency effects.

From Figure 7, it is evident that the reduction in the total interaction energy (approximately 700 kJ mol^{-1} across the halide series for both metals) is almost entirely due to the destabilization in the metal-bridge interaction as fluorine is replaced by its heavier congeners. The reduction in the metal-bridge interaction is observed to mirror approximately the trend in energy associated with the formation of the terminal MX_3 fragments seen in Table 3. The decreasing metal-bridge interaction can therefore be directly attributed to progressively weaker $M-X_{bridge}$ bonding as the halide changes from fluoride through to iodide. Accordingly, the repulsive interactions between the bridging halides do not appear to play an important role in determining the overall stability of the $M_2X_9^{3-}$ unit, at least not in the BS state where the structure corresponds essentially to that of the $S = 0$ state and the bridging halides are relatively far apart because of the compressed geometry of the dimer.

Acknowledgment. Financial support from the Australian Research Council (ARC) to R.S. is gratefully acknowledged.

IC001476M